A Coupling Mechanism for Wind and Waves

WILLIAM PERRIE AND LIANGMING WANG

Physical and Chemical Sciences, Scotia–Fundy Region, Department of Fisheries and Oceans, Bedford Institute of Oceanography, Dartmouth, Nova Scotia, Canada

(Manuscript received 18 February 1994, in final form 11 July 1994)

ABSTRACT

The authors present a simple model for the dynamics that couple the atmospheric boundary layer and wind-generated waves. The model is empirically motivated by parameterizations for the sea state–dependent drag coefficient and sea surface roughness derived by Smith et al. from HEXOS measurements. Estimates are made for the effect the coupling dynamics has on predicted sea state parameters such as spectral wave energy and the air–sea flux of momentum. Results are verified with observations collected during the CAL/VAL experiment of Dobson and Vachon. The authors demonstrate that inclusion of the coupling dynamics systematically improves wave modeling. The effect of the coupling dynamics is particularly important for young waves in the presence of high wind speeds. A tendency to improve estimates of maximum wave heights is achieved.

1. Introduction

In meteorology, the geostrophic wind is used to express the balance relationship between the gravitational potential field and the wind field on a two-dimensional surface. The thermal wind is used to express the balance relationship between the change of wind with height and the mean gradient temperature field in three-dimensional space. A question of considerable interest in both atmospheric and oceanic dynamics, which is as yet unsolved, concerns the balance relationship between the wind profile in the boundary layer and the sea state. To answer this question, it is important to recognize that the key parameter at the air–sea interface, in studies of oceanic and atmospheric dynamics, is the sea surface roughness. Clearly, the sea surface roughness is directly related to the surface waves, which in turn are driven by the wind profile in the atmospheric boundary layer. However, the nonlinearity of the relationship makes it difficult to relate sea surface roughness to wave parameters in a simple quantitative manner. Theoretical approaches have been developed by Chalikov (1993), Chalikov and Belevich (1993), Janssen (1991), and Janssen (1989) but have not yet been applied three-dimensionally. Moreover, though swell remains an important issue, there is no theory, which treats the roughness length in terms of both wind waves and swell, that has been corroborated by field observations. Empirically motivated relations between sea surface roughness and sea state parameters such as wave age have been presented by Geernaert et al. (1987), Donelan (1990), Maat et al. (1991), and Smith et al. (1992). Because empirically motivated relations are much simpler than a more formal analysis, for example, Chalikov and Belevich (1993), they constitute a preliminary approach to coupling winds and waves in three dimensions.

Presently, there is a growing interest in data assimilation in oceanic models, because the launch of a new generation of satellites makes a wealth of sea surface data available, both for the atmosphere and for the ocean. Since remotely sensed marine winds are based on the electromagnetic signature of wind-driven waves on the sea surface, a relationship between wind stress and sea state is of considerable interest. A consistent analysis between the wind and wave fields has been advocated by Janssen (1989), Lionello et al. (1992), and de las Heras and Janssen (1992). For example, they have used the adjoint to a simplified coupled wind–wave model to construct wind and wave fields to minimize a "misfit" function quantifying the difference between observed and modeled wind and wave estimates. Although they have therefore adjusted the wind fields so that the winds are consistent with the waves, it has not been in conjunction with a comprehensive boundary-layer model for sea surface fluxes of momentum, heat, and vapor. A coupled wind–wave model, utilizing a full boundary-layer model and a wave model, allows not only dynamic consistency between wind and wave models but also a consistent approach to data assimilation of both wind and wave fields.

Ultimately, the coupling of the boundary layer with a wave model must result in a derivation of the equilibrium state between winds and waves. "Equilibrium" is understood in terms of implicitly consistent estimates for sea surface roughness in both the boundary-layer

Corresponding author address: Dr. William Perrie, P.O. Box 1006, Bedford Institute of Oceanography, Dartmouth, NS B2Y 4A2, Canada.

model and in the wave model. In weather forecast offices using standard wave models, such as the WAM model of Hasselmann et al. (1988) for example, the wave model is not consistent with the models for the atmospheric boundary layer, in the sense that an "equilibrium state" is not achieved. Three main concerns are involved in the specification of an equilibrium state.

First, given a wind speed V_{10} at a reference height such as 10 m at specific space–time coordinates, the standard wave model uses empirical formulas to produce a friction velocity $\mathcal{U}_*^e$, which in turn is used to estimate spectral wave energy $E(f, \theta)$. However, the wind speed V_{10} is produced by a meteorological boundary-layer model, which involves a friction velocity $\mathcal{U}_*$, drag coefficient C_d, sea surface roughness Z_0, and appropriate thermal conditions. Thus, the friction velocity $\mathcal{U}_*^e$ in the wave model differs from the friction velocity $\mathcal{U}_*$ in the atmospheric model. Second, Z_0 and C_d depend on the wind profile variation with height, rather than simply the wind speed itself at a reference level such as 10 m. The use of empirical formulas to estimate $\mathcal{U}_*^e$ and C_d^e as functions of wind speed V_{10}, implies that Z_0^e and C_d^e in the wave model differ from corresponding estimates Z_0 and C_d in the meteorological model. Finally, the reaction of sea states on the wind profile with height is not taken into account in modern wave models or in operational meteorology. The modification of the wind profile occurs because the interaction between the wind field and wind-generated ocean waves is strong.

In section 2, we present an empirically based model of the sea surface roughness, which is used in coupling ocean waves to the wind fields in a boundary-layer model. The models for waves and the boundary layer are described in section 3. Comparison with results of Janssen (1991) and verification with the observations from the CAL/VAL experiment of Dobson and Vachon (1994) are presented in sections 4–5.

2. Sea surface roughness

The dynamical coupling between the atmosphere and the ocean has been the subject of numerous research efforts in the last few years. Although the effects of some characteristic properties are becoming clearer, the extremely complex processes of air–sea interaction are still not fully understood. The best known relation for the roughness of the sea surface Z_0, proposed by Charnock (1955), states that the sea surface roughness Z_0 depends only on the friction velocity $\mathcal{U}_*$: all characteristics of the wave field are missing,

$$Z_0 = \mathcal{C}_0 \times \left\{\frac{\mathcal{U}_*^2}{G}\right\}, \tag{2.1}$$

where G is the acceleration due to gravity and $\mathcal{C}_0$ is a constant. The constant $\mathcal{C}_0$ has been subjected to considerable revision with the analysis of various sets of field observations. Wu (1980) proposed a value of 0.0185 for $\mathcal{C}_0$ after averaging results from a wide range of datasets. The Charnock relation of Eq. (2.1) is therefore a composite description for sea surface roughness under the varied sea state conditions that can exist. It follows that the Charnock relation is not capable of a good representation of specific dynamical processes, for example, young wind-generated waves or the response of waves to changing (turning) wind directions. A clear demonstration of the breakdown of the Charnock relation, in all but mature wave conditions, was given by Donelan (1982, 1990).

The variation of roughness Z_0 with wave parameters, such as wave age $C_p/\mathcal{U}_*$, where C_p is the phase velocity at the peak of the wave spectrum, has proved elusive to determine. In the analysis of several studies of laboratory and field observations, Toba and Koga (1986) and Toba et al. (1990) combined field data with laboratory data, which appeared to show that Z_0 decreases with decreasing wave age $C_p/\mathcal{U}_*$, according to the relation

$$Z_0 = 0.025\left\{\frac{C_p}{\mathcal{U}_*}\right\}\left\{\frac{\mathcal{U}_*^2}{G}\right\}, \tag{2.2}$$

so that the roughness is in direct proportion to wave age. An alternate relation between Z_0 and wave age $C_p/\mathcal{U}_*$, proposed by Nordeng (1991), is

$$Z_0 = 0.11 \times \left\{\frac{C_p}{\mathcal{U}_*}\right\}^{-3/4} \times \left[1 - e^{-W}\left(1 + \frac{W^2}{2} + \frac{W^3}{6}\right)\right]^{1/2}\left\{\frac{\mathcal{U}_*^2}{G}\right\}, \tag{2.3}$$

where $W = 2\kappa\{C_p/\mathcal{U}_*\}$, and κ is the von Kármán constant. Equation (2.3) suggests that Z_0 achieves a maximum value for $C_p/\mathcal{U}_*$ around 5, corresponding to young waves.

Following the recent HEXOS experiment in the North Sea, Maat et al. (1991) proposed the relation between roughness Z_0 and wave age $C_p/\mathcal{U}_*$:

$$Z_0 = \mu\left(\frac{\mathcal{U}_*^2}{G}\right)\left(\frac{C_p}{\mathcal{U}_*}\right)^n, \tag{2.4}$$

where the Charnock (1958) relation corresponds to $n = 0$ and $\mu = 0.012$, Wu (1980) corresponds to $n = 0$ and $\mu = 0.0185$, Toba and Koga (1986) correspond to $n = 1$ and $\mu = 0.025$, and Hsu (1974, 1986) corresponds to $n = -1/2$ and $\mu = 0.90$. In a review of several published datasets, Donelan (1990) normalized Z_0 by significant wave height H_s, which in terms of the total energy E_0, is

$$H_s = 4.0\sqrt{E_0}, \tag{2.5}$$

and E_0 is obtained by integrating the 2-dimensional spectral wave energy $E(f, \theta)$ over all frequency f and directional θ bands [as specified later in Eq. (3.12)].

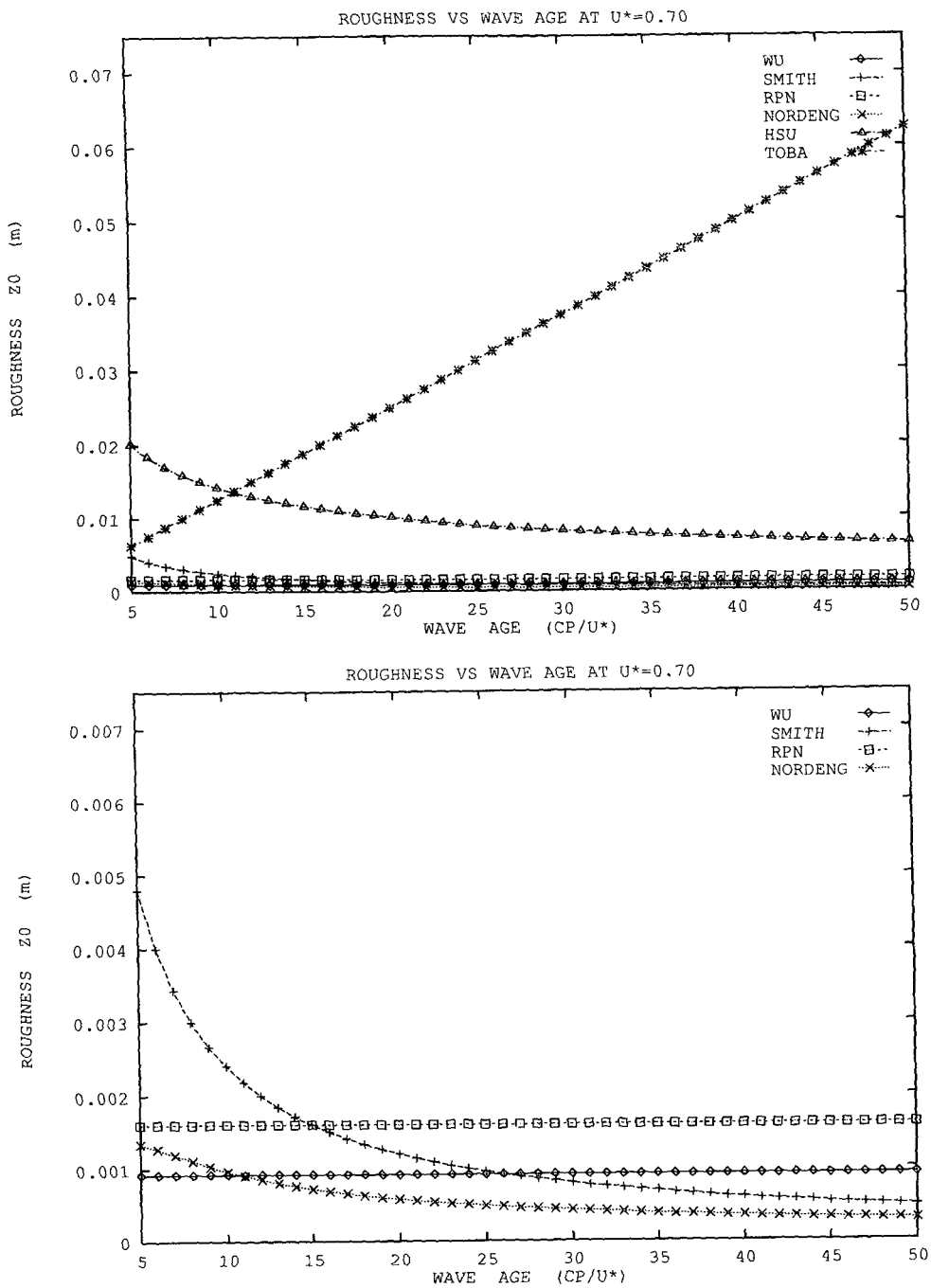

FIG. 1. (a) Variation of sea surface roughness with wave age as parameterized by Wu (Charnock), Smith, RPN, Nordeng, Hsu, and Toba. (b) With expanded scale, without Toba or Hsu.

He calculated the ratio Z_0/H_s as a function of wave age $C_p/\mathcal{U}_*$ and found that $n \approx -1$. Finally, Smith et al. (1992) recently completed corrections to the HEXOS data for flow distortion with the result $\mu = 0.48$, in place of the earlier estimate by Maat et al. (1991).

A comparison of the aforementioned roughness formulations Z_0 is given in Figs. 1a,b. In these figures, the Charnock relation (2.1) using the Wu (1980) coefficient $\mathcal{C}_0 = 0.0185$ is denoted "WU." The Canadian operational boundary-layer model at RPN (Recherche en Prévision Numérique, Dorval, Québec) uses the Charnock relation (2.1) with $\mathcal{C}_0 = 0.032$. Of all the relations shown in Fig. 1a, the Toba et al. (1990) result is extraordinary in that, for a fixed wind stress, older waves are rougher than younger waves. The Toba et

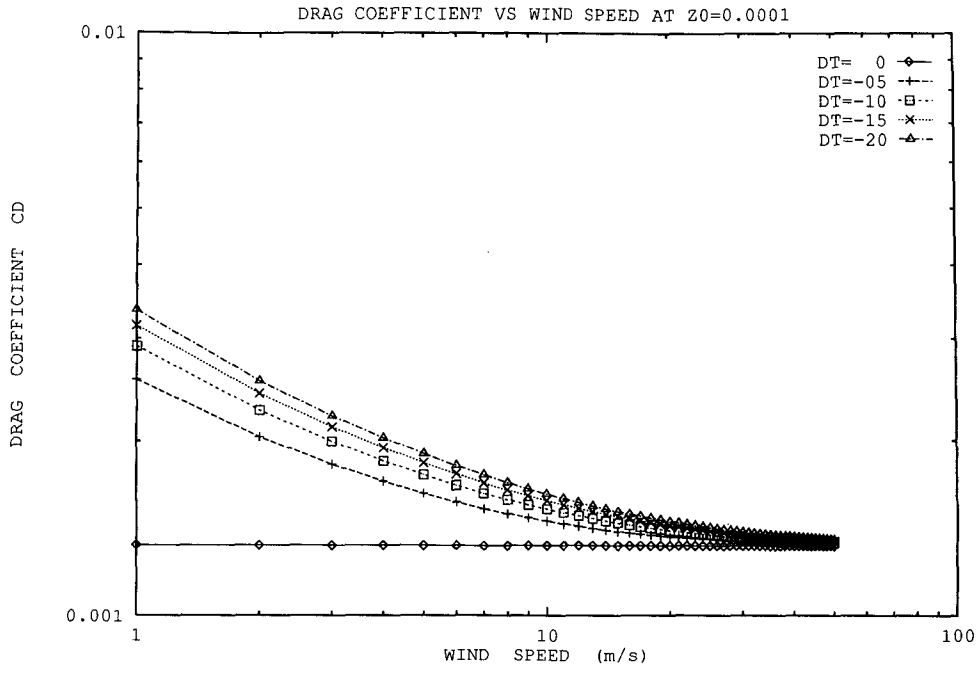

FIG. 2. Boundary-layer model estimates for the variation of the drag coefficient C_d with wind speed at various air–sea temperature differences ΔT, with $Z_0 = 0.0001$.

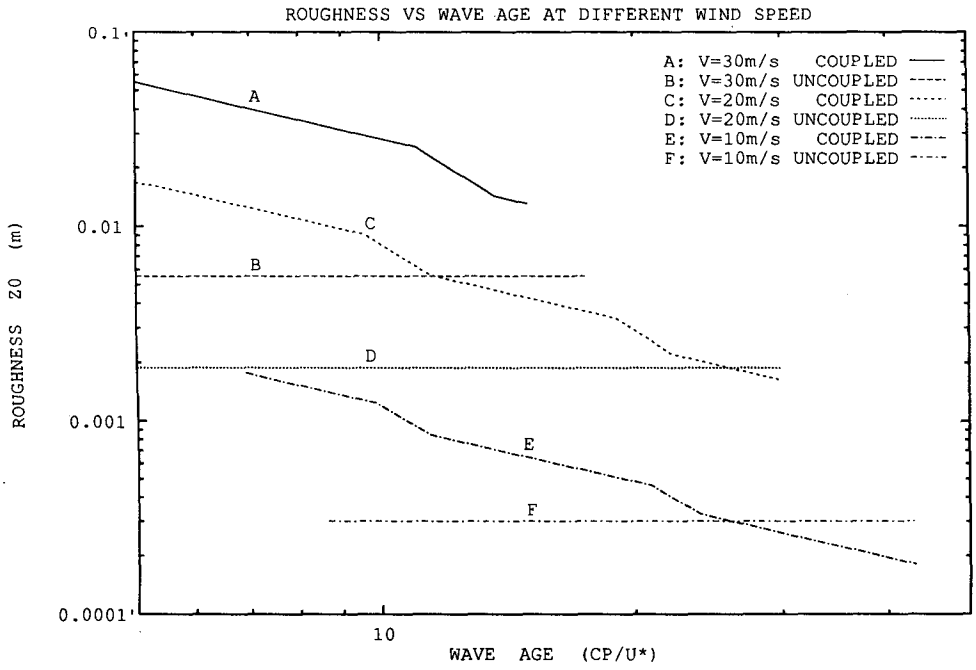

FIG. 3. Comparison of coupled and uncoupled model estimates (a) for the variation in roughness Z_0 with wave age for various wind speeds, and (b) for the drag coefficient C_d for young waves (‡) with the estimates from Janssen (1991). Symbols of Janssen (1991): (□) $10 < C_p/U_* < 15$, (+) $15 < C_p/U_* < 20$, (◇) $20 < C_p/U_* < 25$, and (△) $C_p/U_* > 25$. (c) Comparison of drag coefficients (□, +, and ◇) from Fig. 11 after Smith et al. (1992) with estimates from the coupled model at wind speeds $V = 5$, 10, and 20 m s^{-1}.

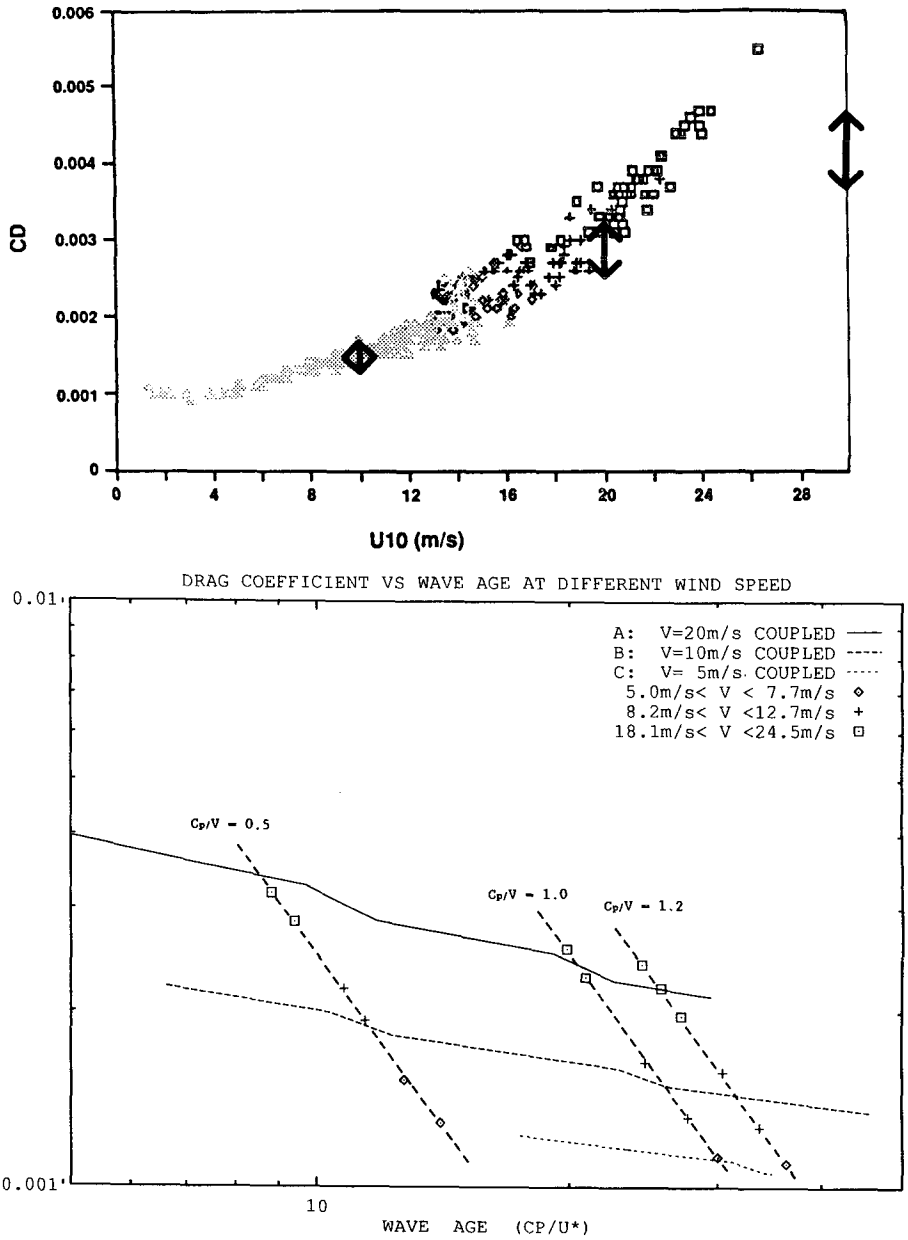

FIG. 3. (*Continued*)

al. (1990) result has been disputed by Donelan et al. (1993); the Hsu (1974, 1986) result in Fig. 1a is also anomolous. Although the Hsu (1974, 1986) roughness Z_0 decreases with increasing $C_p/\mathcal{U}_*$, the roughness Z_0 is always greater than that of the Charnock (1955) relation, (2.1), which had support from field data. Finally, the Nordeng (1991) result is always less than Charnock's relation (2.1), except when the wave age $C_p/\mathcal{U}_*$ is less than 10. Further discussion of relations between roughness Z_0 and wave age $C_p/\mathcal{U}_*$ is given in Maat et al. (1991) and Donelan et al. (1993).

The remainder of this paper concerns, on one hand, Wu's (1980) version of the Charnock relation (2.1), which is independent of sea state, and is hereafter denoted as uncoupled. On the other hand, we are concerned with the Smith et al. (1992) wave age $C_p/\mathcal{U}_*$ dependent roughness Z_0, expressed as

$$Z_0 = 0.48 \times \left\{\frac{C_p}{\mathcal{U}_*}\right\}^{-1}\left\{\frac{\mathcal{U}_*^2}{G}\right\}, \qquad (2.6)$$

which has explicit dependency on sea state maturity. Hereafter we denote Eq. (2.6) as coupled. Both Wu

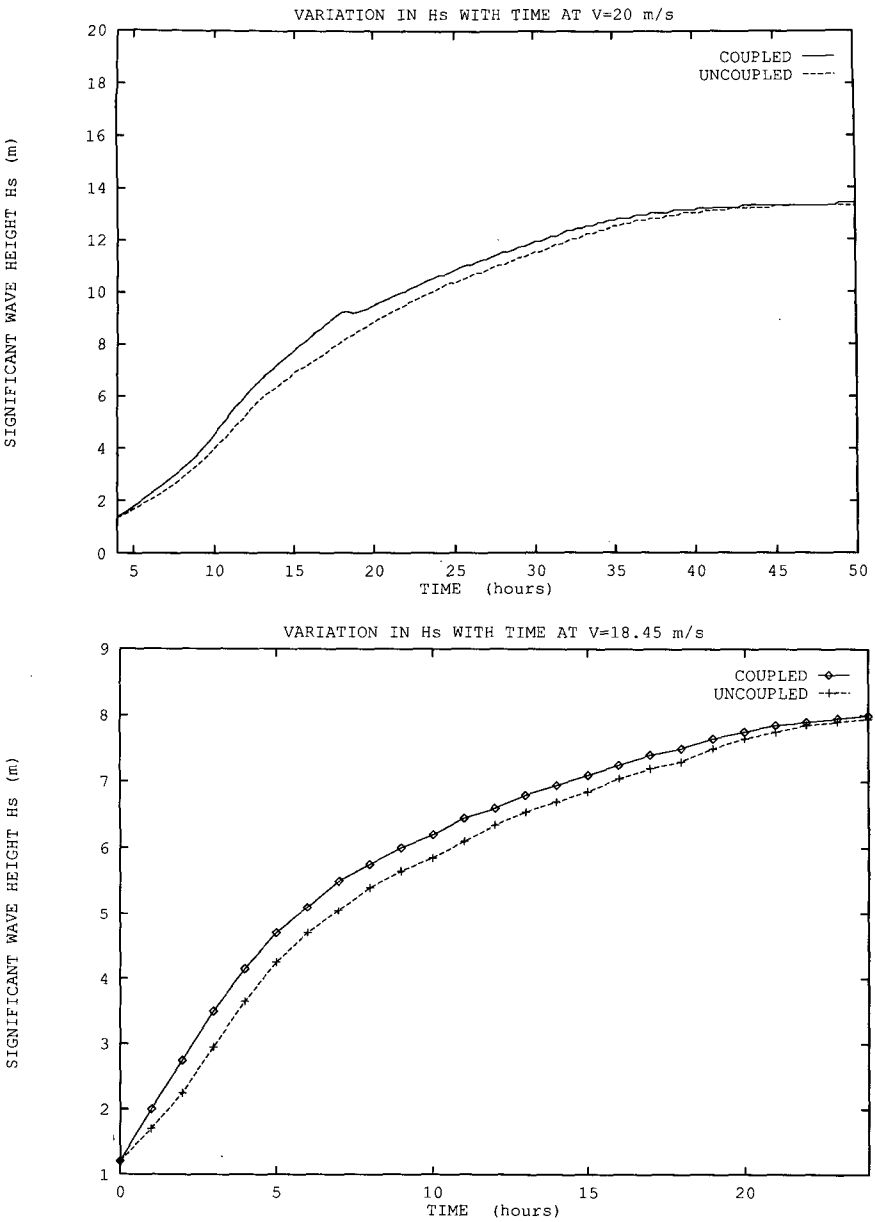

FIG. 4. Comparison of uncoupled (dashed) and coupled (solid) model estimates for H_s as a function of time at (a) a wind speed of 20 m s^{-1} and (b) after Janssen (1991) at wind speed 18.45 m s^{-1}.

(1980) and Smith et al. (1992) formulations constitute results based on observations. Moreover, with respect to the HEXOS measurements, the rms error of the Smith et al. (1992) formulation (2.6) is less than the rms errors from normalized $Z_0/\sqrt{E_0}$ formulations suggested by Donelan et al. (1993). From Fig. 1b, the coupled model intersects the uncoupled model at wave age $C_p/\mathcal{U}_* \approx 26$, whereas the intersection with RPN occurs at $C_p/\mathcal{U}_* \approx 15$. The RPN model is therefore tuned for young waves as compared to the more mature sea state implicit in the Wu (1980) constant.

3. Boundary-layer and wave models

a. Boundary-layer model

The boundary-layer model used in this study is quite similar to the Canadian operational boundary-layer model, as documented by Delage (1988a,b). It is a diagnostic model, in that given the wind speed and the roughness Z_0, it specifies boundary-layer parameters at a given grid point. The vertical fluxes of momentum, sensible heat, and latent heat are computed at the surface (denoted by subscript s) and may be written as

TABLE 1. Estimated significant wave height H_s (in meters) under neutral conditions as a function of time and wind speed V_{10} for coupled and uncoupled models.

	Wind speed V_{10} (m s^{-1})			
	Uncoupled		Coupled	
Time (h)	10	20	10	20
10	1.39	3.95	1.68	4.49
20	1.95	8.71	2.10	9.35
30	2.22	11.30	2.31	11.70
40	2.40	12.90	2.47	13.00
50	2.54	13.30	2.60	13.30

$$\overline{|w'V'|}_s = (C_M|V_a|)^2 \quad (3.1)$$

$$\overline{(w'T')}_s = c_p C_M C_T |V_a|(T_s - T_a) \quad (3.2)$$

$$\overline{(w'q')}_s = LC_M C_T |V_a|(q_s - q_a), \quad (3.3)$$

where the transfer coefficients for momentum and heat, denoted C_M and C_T, are functions of the bulk Richardson number Ri_b, anemometer level Z_a, and roughness Z_0. Latent heat is denoted by L and specific heat at constant pressure by c_p. Air temperature is denoted T_a, and sea surface temperature T_s. The specific heat content of water vapor at the sea surface is denoted q_a, and specific heat content of liquid water is q_s. Details relating C_M and C_T to Ri_b, Z_0, the thermal roughness Z_{0T}, and other variables are given in the appendix.

It is important to note that this boundary-layer model implies that the drag coefficient C_d depends on the roughness Z_0 under neutral conditions, satisfying the usual relation

$$C_{dn} = \left(\frac{\mathcal{U}_*}{U_z}\right)^2 = \left\{\frac{\kappa}{\ln\left(\frac{Z_0 + Z_a}{Z_0}\right)}\right\}^2, \quad (3.4)$$

rather than the wind speed at a desired anemometer level Z_a. The problem is that many empirical relations attempt to relate the drag coefficient or roughness to wind speed only without considering sea state. An example is from Hsu (1986):

$$C_{d10} = \left\{\frac{0.4}{14.56 - \ln V_{10}}\right\}^2, \quad (3.5)$$

which implies that the neutral drag coefficient is uniquely a function of wind speed. Numerous empirical relationships between the neutral drag coefficient and wind speed have been proposed. Donelan (1990) and Donelan et al. (1993) pointed out that the development of these relationships is due to differences in sea state during various experimental situations.

In our boundary-layer model, the drag coefficient is a function not only of the vertical wind profile but also of the sea state roughness Z_0. The coefficient of heat exchange $C_M C_T$ [as seen in Eqs. (3.2) and (3.3)] may also be shown to be a function of roughness Z_0 under near-neutral conditions. Figure 2 shows the change in drag coefficient C_d with wind speed at various temperature differences under unstable conditions with constant $Z_0 = 0.0001$ (m), corresponding to $C_{dn} \approx 10^{-3}$. It is evident that C_d is largely insensitive to the magnitude of the temperature differences at high winds. Increasing the roughness Z_0 with wind speed, as in the Charnock relation (2.1), causes the high wind speed asymptote in Fig. 2 to also increase, as shown in Smith (1988). It may also be shown that at high wind speeds, the coefficient of heat exchange $C_M C_T$, the friction velocity $\mathcal{U}_*$, and the flux of momentum FM, are largely insensitive to the magnitude of the temperature differences. Concomitantly, the flux of sensible heat FS may be shown to be sensitive to temperature differences at all wind speeds, as presented in Wang and Perrie (1993).

b. *Wave model*

The spectral energy density for surface gravity waves in deep water $E(f, \theta)$ evolves in space and time according to the relation

$$\frac{\partial E(f,\theta)}{\partial t} + \mathfrak{c}_g \cdot \nabla E(f,\theta) = \varphi_{\mathrm{in}} + \varphi_{\mathrm{nl}} + \varphi_{\mathrm{ds}}, \quad (3.6)$$

where φ_{in} is the spectral energy input by the wind, φ_{ds} is the dissipation due to wave breaking and white cap formation, and φ_{nl} is the change in spectral energy due to nonlinear transfer resulting from wave–wave interactions. The wave model constitutes an integration of the spectral energy balance equation (3.6) in space and time. We use the WAM model of Hasselmann et al. (1988).

Parameterizations for wind input energy φ_{in} are heavily motivated by the observations of Snyder et al. (1981). The form is

$$\varphi_{\mathrm{in}} \approx \beta E(f,\theta), \quad (3.7)$$

where β, as specified by Hasselmann et al. (1988), is given by

$$\beta = \max\left\{0, 0.25\,\frac{\rho_a}{\rho_w}\left(28\,\frac{\mathcal{U}_*}{\zeta}\cos\theta - 1\right)\right\}\omega, \quad (3.8)$$

and ρ_a and ρ_w are air and water densities. The friction velocity in the wave direction is $\mathcal{U}_* \cos\theta$, with θ the direction of the wind relative to the wave propagation direction. Phase velocity is $\zeta = \omega/k$, and angular frequency ω is related to wavenumber k through the deep water dispersion relation.

Dissipation due to wave breaking φ_{ds} is assumed to have a simple form, motivated by Hasselmann (1974), as well as numerical experiments reported in Hasselmann et al. (1988), and may be written as follows:

$$\varphi_{\mathrm{ds}} \approx gk^{-4}\mathcal{F}(k^4 F(\mathbf{k})), \quad (3.9)$$

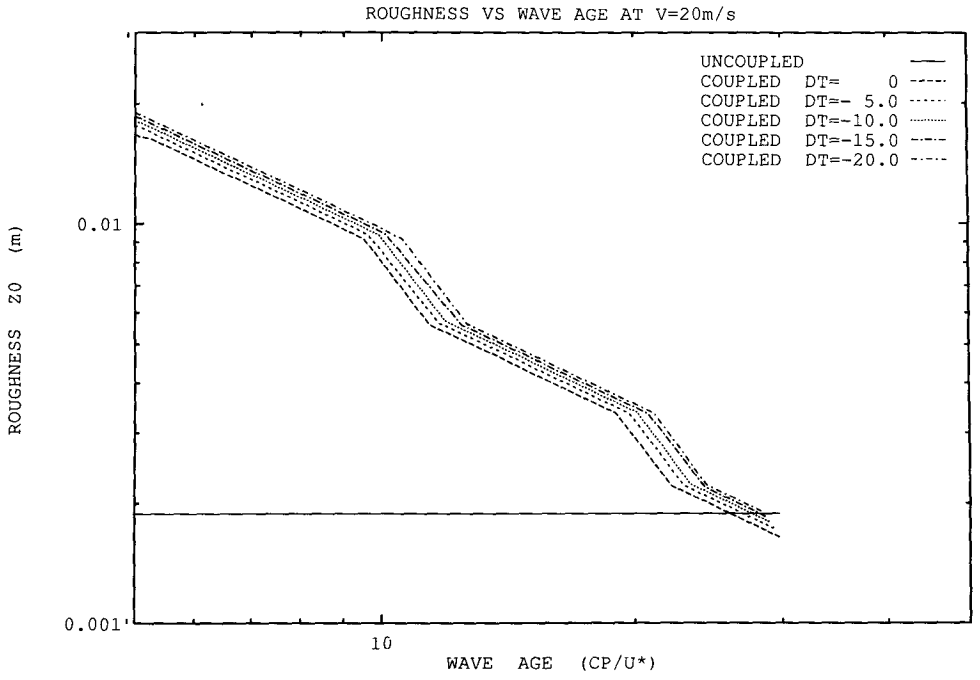

FIG. 5. (a) Comparison of uncoupled and coupled model estimates for Z_0 as a function of wave age at wind speed 20 m s^{-1}, and as a function of air–sea temperature differences DT. (b) Variation of H_s, as estimated from the uncoupled model, with time as a function of DT and DQ for wind speed of 20 m s^{-1}. (c) As in (b) but for the coupled model.

where $k = |\mathbf{k}|$, $F(\mathbf{k})$ is the energy spectrum in vector wavenumber space $\mathbf{k}$, and $\mathcal{F}$ is an appropriate functional. It is usually taken as

$$\mathcal{F} = -2.33 \times 10^{-5}\hat{\omega}\left(\frac{\omega}{\hat{\omega}}\right)^2\left(\frac{\hat{\alpha}}{\hat{\alpha}_{pm}}\right)^2 E(f, \theta), \quad (3.10)$$

where

$$\hat{\omega} = \left(E_0^{-1}\int\int E(f, \theta)\omega^{-1}dfd\theta\right)^{-1} \quad (3.11)$$

$$\hat{\alpha} = E_0\hat{\omega}^4 g^{-2}, E_0 = \int\int E(f, \theta)dfd\theta, \quad (3.12)$$

and

$$\hat{\alpha}_{pm} = \frac{2}{3}E_0 g^{-2} \times \left(E_0^{-1}\int\int E(f, \theta)\omega dfd\theta\right)^4\Big|_{\text{Pierson–Moskowitz}} \approx 0.003. \quad (3.13)$$

The complete representation for nonlinear transfer due to wave–wave interactions φ_{nl}, in terms of a sixfold Boltzmann integral in wavenumber space, was given by Hasselmann (1962):

$$\mathcal{F}_{nl}(\mathbf{k}_1) = \int\int\int \zeta^2(\mathbf{k}_1, \mathbf{k}_2, \mathbf{k}_3, \mathbf{k}_4) \times \mathcal{D}(\mathbf{k}_1, \mathbf{k}_2, \mathbf{k}_3, \mathbf{k}_4)\delta(\mathbf{k}_1 + \mathbf{k}_2 - \mathbf{k}_3 - \mathbf{k}_4) \times \delta(\omega_1 + \omega_2 - \omega_3 - \omega_4)d\mathbf{k}_2 d\mathbf{k}_3 d\mathbf{k}_4. \quad (3.14)$$

The WAM model approximation to Eq. (3.14) is described in Hasselmann et al. (1988) and is based on the so-called discrete interaction approximation.

In implementing the parameterizations of Eqs. (3.7)–(3.14) and integrating the energy balance equation (3.6), the two-dimensional wave spectrum $E(f, \theta)$ is represented by 54 frequencies and 12 directions for a total of 648 spectral elements at every grid point. The 54 frequencies range from 0.0417725 to 0.65268 Hz, increasing in geometric progression with a constant ratio of 1.1. The 12 directional bands each have a width of 30°.

4. Coupled wind–sea model

The coupled and uncoupled roughness parameterizations of section 2, the boundary-layer model of section 3a, and the wave model of section 3b are connected together iteratively. At a given time step, we first use the wind speed and direction (which are specified externally as forcing for the coupled boundary layer–wave model dynamics), to compute the peak frequency f_p from the wave model. Assum-

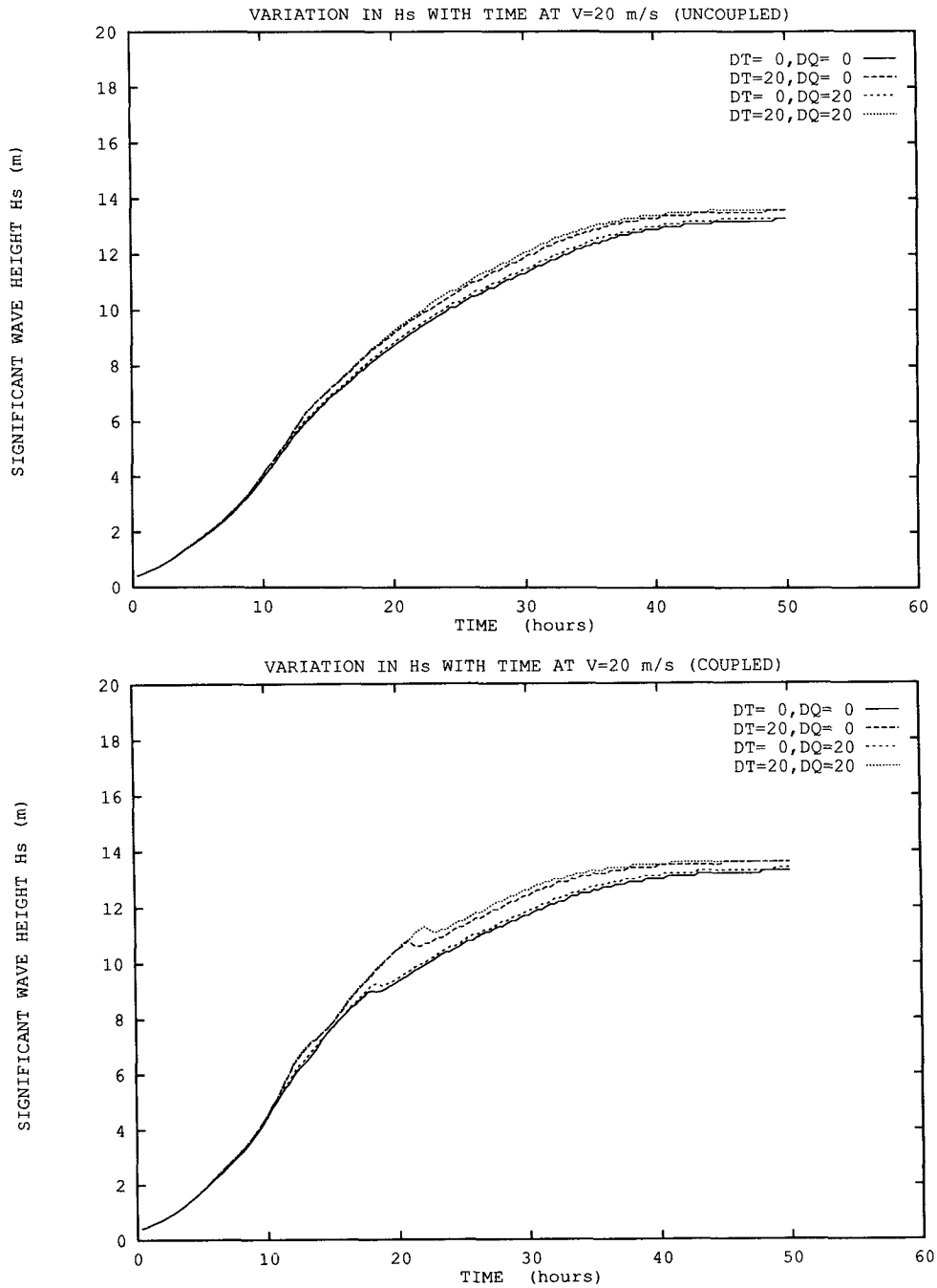

FIG. 5. (*Continued*)

ing a first guess roughness Z_0, the friction velocity $\mathcal{U}_*$ and the drag coefficient C_d are then obtained from the boundary-layer model. Thereafter a "new" roughness is calculated using either the Charnock formula (2.1) in the uncoupled model or the Smith et al. (1992) formulation of (2.6) in the coupled model. If the new roughness is within allowable error relative to the previous roughness, we proceed to the next time step in the simulation. Otherwise we must iterate, and using C_d, $\mathcal{U}_*$, and the wave model, we must recompute the peak frequency f_p. The boundary-layer model then leads to a new estimates for C_d and $\mathcal{U}_*$. Thence, (2.1) or (2.6) lead to a revised estimate of the roughness. When the iteration process converges, with respect to an allowable relative error, we proceed to the next time step of the simulation.

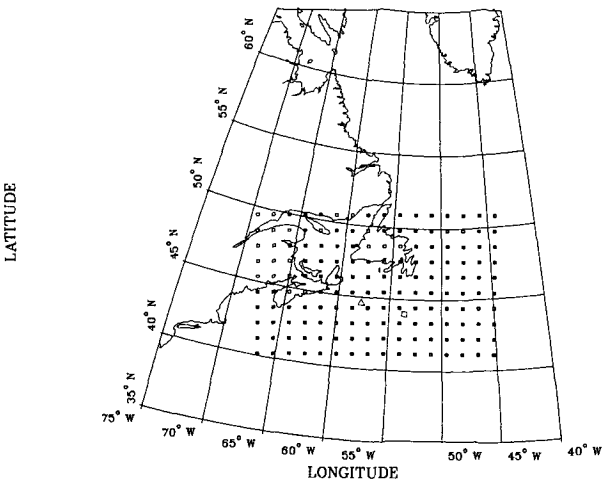

FIG. 6. Grid points for implementation of the wave and boundary-layer models for verification with CAL/VAL measurements. Operational buoys are buoy 44138 (△) and buoy 44139 (□).

Figure 3a shows the change of roughness Z_0 with wave age at different wind speeds for both coupled and uncoupled models. Results from the coupled model show that the roughness Z_0 decreases with increasing wave age given a constant wind speed. Moreover, both the coupled and the uncoupled models show that Z_0 is not directly proportional to the wind speed. As discussed in section 3a, the drag coefficient C_d is a function of only roughness Z_0, under the neutral conditions of Fig. 3a. Therefore, in the coupled model, C_d changes with changing Z_0, even when the wind speed remains constant.

The intersection of Z_0 from the uncoupled model, with Z_0 from coupled model, occurs at a wave age $C_p/\mathcal{U}_* \approx 26$ in Fig. 3a. This was also evident in Fig. 1b. Wave age ($\approx$26) corresponds to about 5 h at wind speed V_{10} = 10 m s^{-1}, 10 h at V_{10} = 20 m s^{-1}, and (estimated) 15 h at V_{10} = 30 m s^{-1}. No intersection is evident in the V_{10} = 30 m s^{-1} case, because the frequency discretization has a lowest frequency of 0.0417725 Hz, which is not low enough to allow the spectra to evolve to a point where a crossover between coupled and uncoupled models can occur.

The intersections between coupled and uncoupled models at a wave age $C_p/\mathcal{U}_* \approx 26$ indicate that the Charnock relation of Eq. (2.1) corresponds to mature wind wave conditions during high wind situations in the coupled model. This is consistent with the suggestion of Donelan (1982), that the Charnock (1955) relation is only valid for field observations under mature conditions. It is notable that the coupled drag coefficient compares well with Janssen (1991), as shown in Fig. 3b. A further indication that the coupled model estimates are consistent with field data follows from Fig. 3c. Estimated error bars are ±20% on Smith et al. (1992) data in Fig. 3c.

Figure 4a compares significant wave heights H_s as a function of time, as estimated by the coupled and uncoupled models, for wind speed V_{10} = 20 m s^{-1}. Neutral stratification is assumed. Differences in H_s between coupled and uncoupled models are comparable to results presented by Janssen (1991) in Fig. 4b for V_{10} = 18.45 m s^{-1}. Table 1 shows that winds of 20 m s^{-1} produce a maximum difference in H_s of about 14% of the estimated H_s from the uncoupled model after 10 h.

The results shown in Figs. 3–4 and Table 1 assume neutral stratification. The variation in Z_0 with wave age for the uncoupled and the coupled models under a variety of air–sea temperature differences, denoted by "DT," are shown in Fig. 5a. It is evident that Z_0 is slightly sensitive to DT. Differences in estimated significant wave heights H_s between uncoupled and coupled models also exist. Figures 5b and 5c show the evolution of H_s as a function of time, given a wind speed V_{10} of 20 m s^{-1} for different values of DT and DQ ($\equiv q_s - q_a$). Maximum differences are about 15%.

Although a given reference wind speed may be specified as constant in these tests and it is implicit that as the roughness and friction velocity evolve and the sea state matures, the vertical wind profile also changes in time. This is evident in the coupled model and is the subject of a related paper. Of course, the vertical wind profile does not change in the uncoupled model, because changes of roughness and friction velocity do not occur.

5. Model verification: The CAL–VAL experiment

Integrating the full spectral energy balance equation (3.6) leads to a full three-dimensional coupled boundary layer–wave model. To provide model verification using observed field data, implementation was made on the northwest Atlantic on a transverse Mercator projection with an assumed equator at 51°W and a grid spacing of 119 km near Halifax, Nova Scotia. The grid consists of 160 points, of which 139 are water points, at which model parameters are generated as shown in Fig. 6. Two operational wave buoys are located in this grid as shown.

Observations used to verify the model were collected during the CAL/VAL experiment of Dobson and Vachon (1994). Wind data was provided every three hours for the CAL/VAL period (8 to 25 November 1991) by RPN and linearly interplated to hourly wind fields. The time step is 20 minutes for the one-dimensional model and 1 h for three-dimensional model. The buoy data were provided by the Atmospheric Environment Service (AES) in Bedford, Nova Scotia.

a. The 1D model

For a very large ocean, advective effects are not present in observations at very long fetch ($\geqslant 10^3$ km). We may assume that

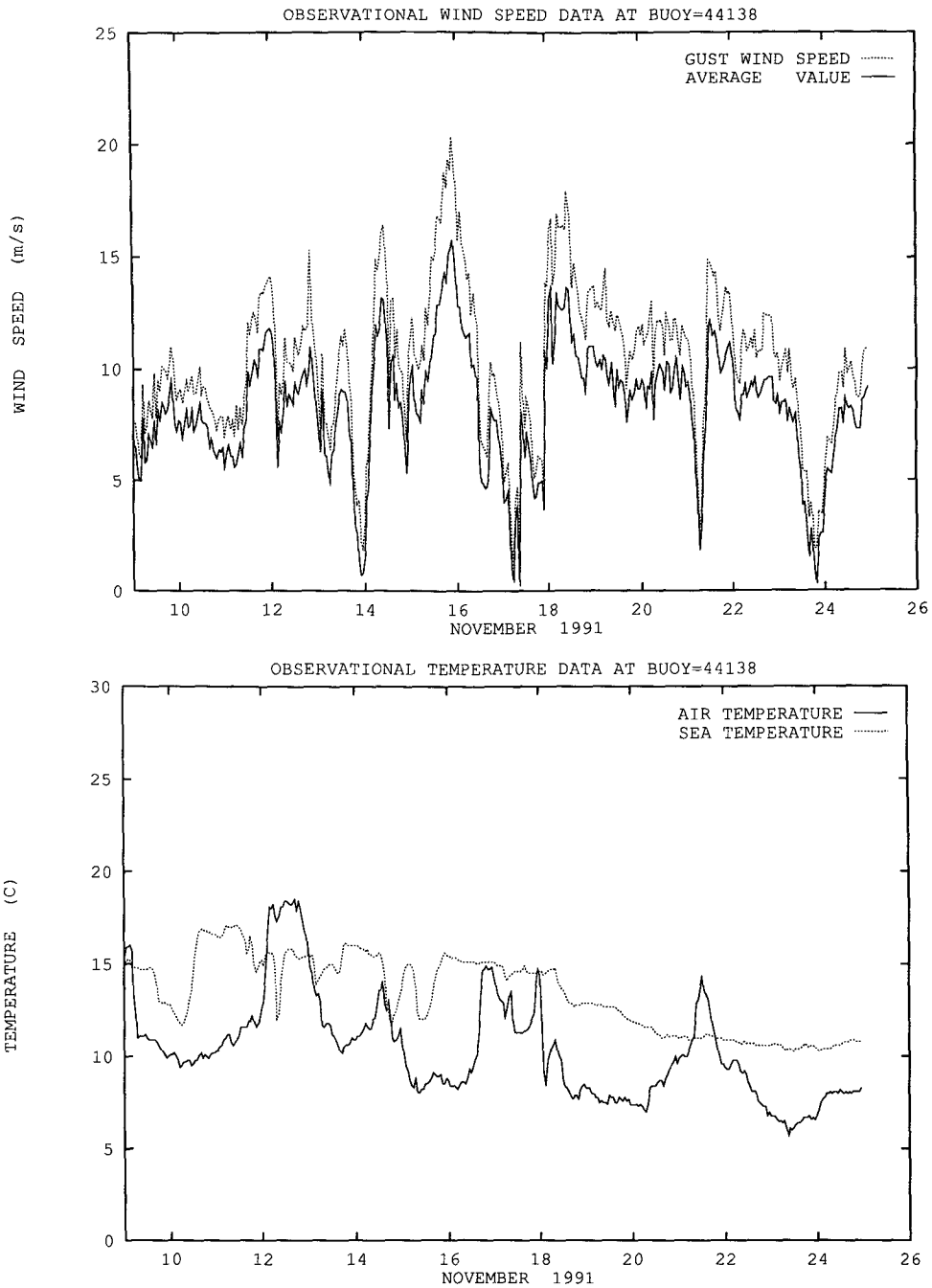

FIG. 7. Time series of (a) average wind speed and gust wind speed and (b) sea temperature (dashed) and air temperature (solid) at wave buoy 44138 during the CAL–VAL experiment.

$$\mathbf{C}_g \cdot \nabla E(f, \theta) \ll \varphi_{\text{in}} + \varphi_{\text{nl}} + \varphi_{\text{ds}}, \qquad (5.1)$$

which implies that Eq. (3.6) may be written as follows:

$$\frac{\partial E(f, \theta)}{\partial t} \approx \varphi_{\text{in}} + \varphi_{\text{nl}} + \varphi_{\text{ds}}, \qquad (5.2)$$

for growing wind sea spectra at long fetch. It is therefore possible to have one-dimensional coupled and uncoupled models for duration-limited waves, evolving in response to forcing by wind from some initial time. Such simple one-point models are important in exploring the basic characteristics of coupled and uncoupled models.

In this section we consider implementation of the one-dimensional coupled and uncoupled models at the wave buoy positions shown in Fig. 6. That is, we neglect

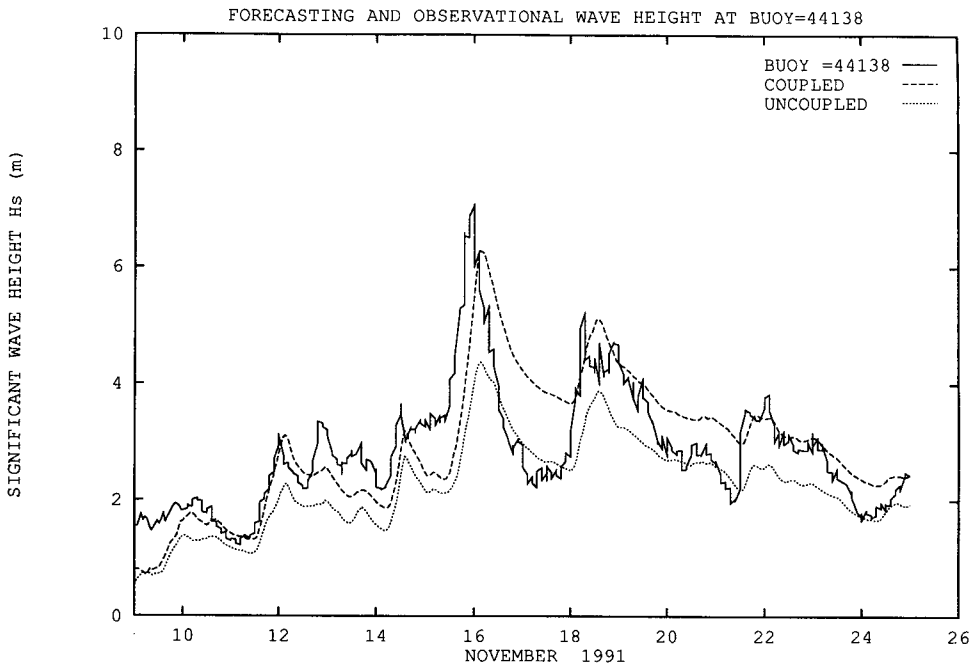

FIG. 8. As in Fig. 7a for measured H_s, and estimated H_s from both coupled and uncoupled models.

advective effects and assume that the approximation of Eq. (5.1) is valid. Figures 7a,b show the time series at buoy 44138 for winds and temperatures. Figure 8 compares observed significant wave heights H_s with estimated H_s from the uncoupled and coupled models. Clearly, both models underestimate the wave heights, but values estimated for H_s from the coupled model are systematically closer to the observations than H_s from uncoupled model. Corresponding results for buoy 44139 are similar.

b. *Three-dimensional verification*

Verification in three dimensions is achieved by integrating the full balance equation (3.6) without the approximation of Eq. (5.1), neglecting advective effects. During the CAL/VAL period a cyclone developed in the region between Nova Scotia and Newfoundland on 15 November. Wind fields for 0000 UTC 15 and 16 November are shown in Figs. 9a,b. Corresponding estimates for significant wave

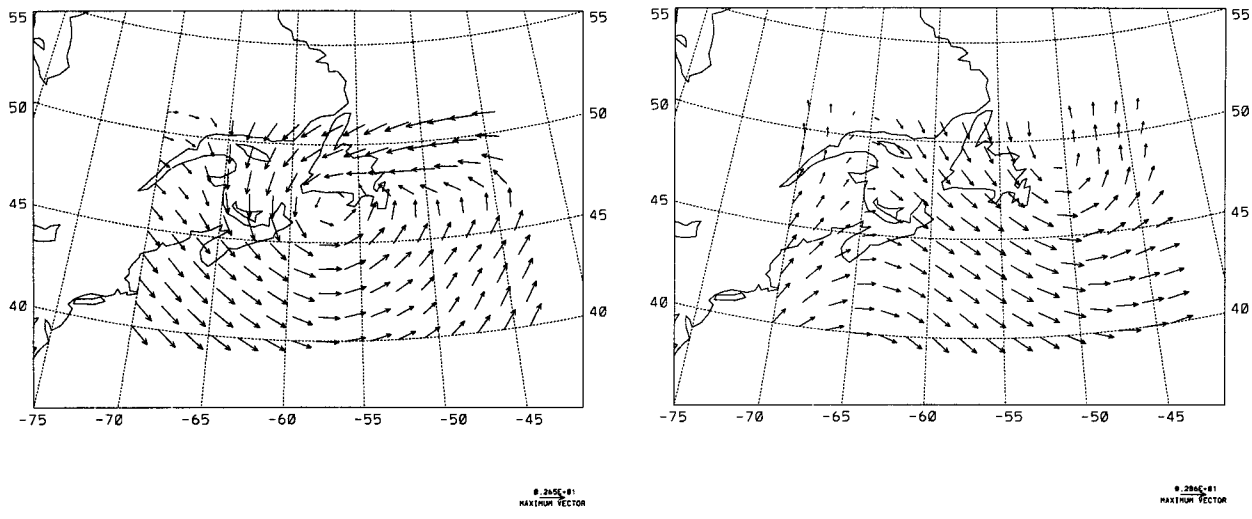

FIG. 9. The wind velocity field at 0000 UTC on (a) 15 November 1991 and (b) 16 November 1991.

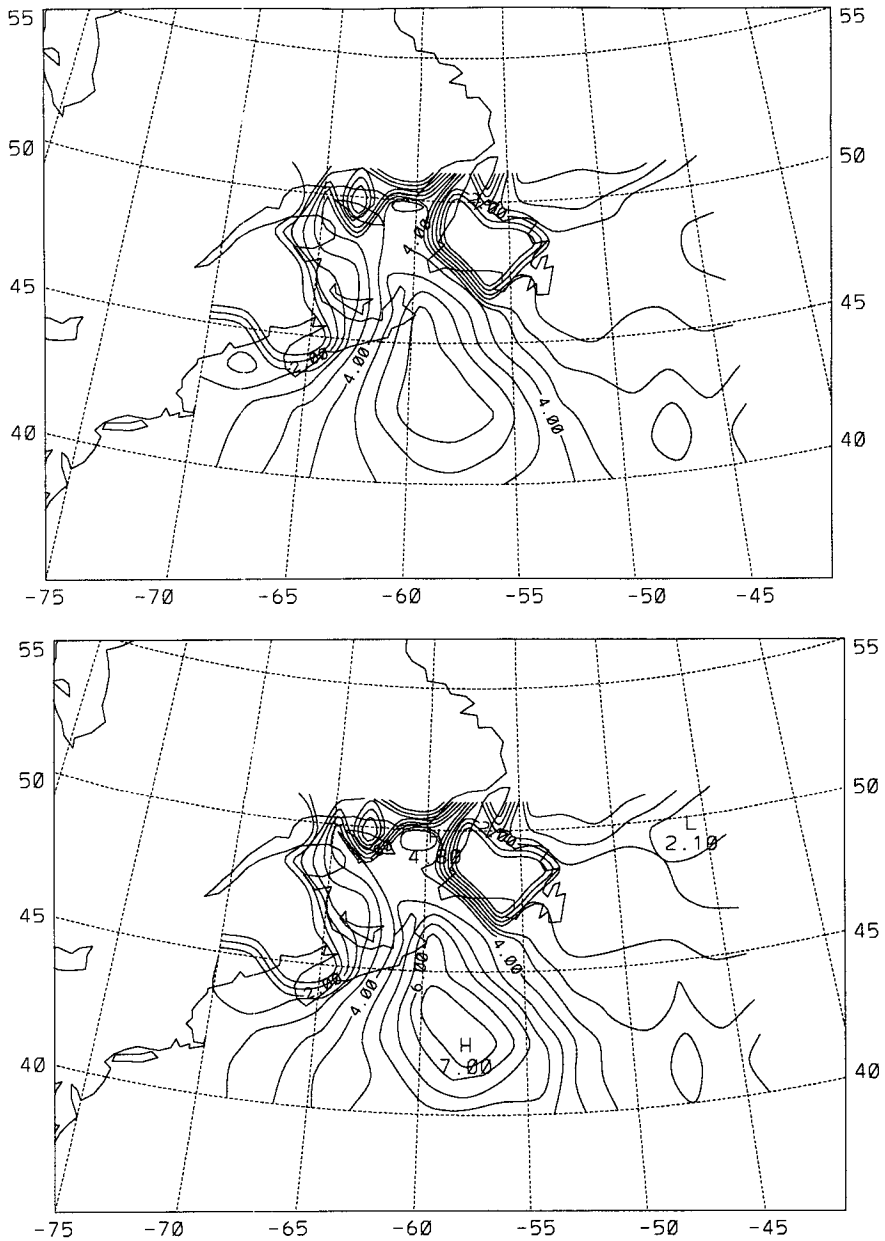

FIG. 10. Contours for H_s at 0000 UTC 16 November 1991 as estimated from (a) the uncoupled model and (b) the coupled model.

height H_s fields for 0000 UTC 16 November for the uncoupled and the coupled models are shown in Figs. 10a,b, respectively. It is notable that the maximum H_s reported by the coupled model is 7.0 m, whereas the uncoupled model reported a maximum H_s of only 5.9 m. The corresponding maximum H_s in the cyclone region, where the wind direction and wind speed are changing rapidly and the wave age is very young, was 7.1 m at buoy 44138, as shown in Fig. 11. This is in good agreement with the coupled model estimate. In other regions of Figs. 10a,b, because the wave age is older, the estimated H_s for the coupled model is almost the same as that of the uncoupled model.

Estimated H_s time series at the model grid point nearest buoy 44138 are shown in Fig. 11, for both the coupled and uncoupled models. It is therefore demonstrated that at the peak of the storm, late on 15 November, the coupled model estimates for H_s are notably closer to measured H_s values than those of the uncoupled model. Lower sea state conditions are less determinate. When observed wave heights

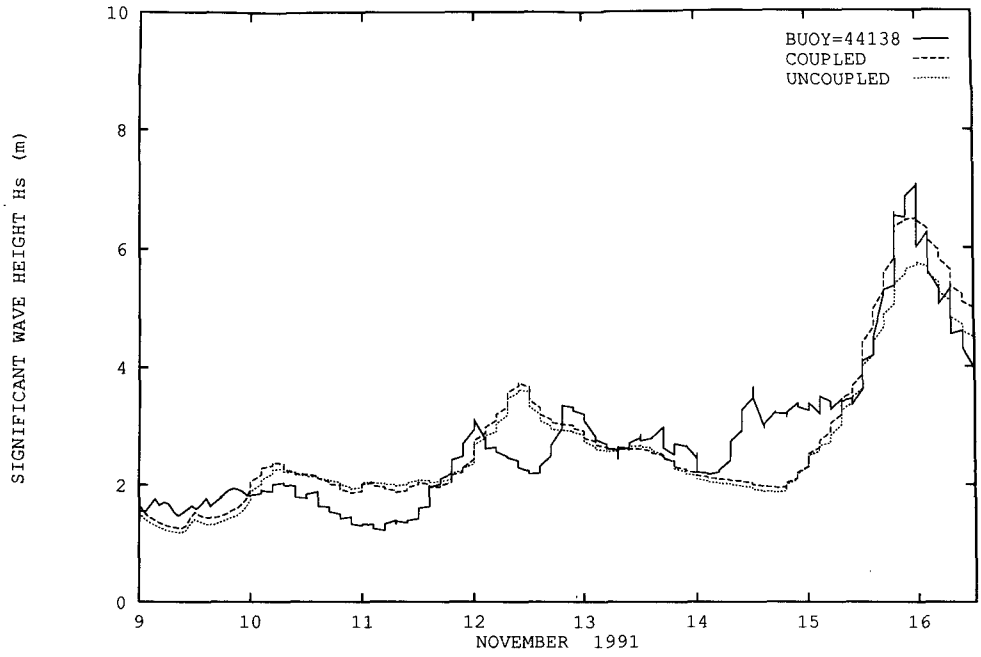

FIG. 11. Time series of H_s as measured at buoy 44138 during CAL/VAL and as estimated from the coupled and uncoupled models.

H_s are in the range 2–3 m during 12–15 November, errors of up to 1.7 m occur. This is not too serious because, whereas a fine-mesh wave model with high quality wind fields and more detailed physics may succeed in modeling these waves of 2–3 m, we are using wind fields from an operational weather forecasting laboratory, a comparatively large grid, and the operational WAM model of Hasselmann et al. (1988). Thus, it is hardly surprising that these waves of 2–3 m are not resolved. Results for buoy 44139 are not shown because the maximum peak values were not as high.

6. Concluding discussion

The standard approach to modeling ocean waves and the atmospheric boundary layer assumes a Charnock relation such as Eq. (2.1), which presupposes that the waves are mature. The corresponding wave age $C_p/\mathcal{U}_*$ is very old. In this approach, the atmospheric boundary layer is uncoupled from the sea state. On the other hand, parameterization of wind wave maturity using variables such as wave age in specifying sea surface roughness Z_0 is achieved in the HEXOS results of Smith et al. (1992). This parameterization is the basis of our coupled model.

If the wind speed is not strong, the difference between estimated H_s provided by the coupled and the uncoupled models is negligible, because the wind waves quickly become mature. However, if the wind speed is strong ($V_{10} \geq 20$ m s^{-1}) the waves take longer to mature and the reaction of the sea state on the boundary layer is important. Inclusion of the coupling dynamics has a significant impact on wave forecasts in this case. The impact is accentuated during unstable conditions.

The HEXOS wave age–dependent drag coefficient of Smith et al. (1992), as implemented in the coupled model, gives a higher wind stress and a more rapid initial growth for young waves. Using an advanced wave model, we have demonstrated that this results in an ability to correct the (WAM model) tendency to underestimate peak values for significant wave height H_s during high sea state conditions. It is significant that this was achieved using the analysis winds from an operational weather forecast office rather than kinematically analyzed wind fields, specifically created for the experiment.

Acknowledgments. The Federal Panel on Energy Research and Development (PERD) and the Northern Cod Fund of Canada provided funding for this research. We are very grateful to Yves Delage for the essential elements of the RPN boundary layer model. We also acknowledge anonymous reviewers for important contributions to this paper.

APPENDIX

Boundary-Layer Model

Under stable conditions, the transfer coefficients can be written as

$$C_M = \frac{\kappa}{\zeta_a} F_M \tag{7.1}$$

$$C_T = \frac{\kappa}{\zeta_a} F_T, \tag{7.2}$$

where

$$\zeta_a \equiv \ln\left(\frac{Z_a + Z_0}{Z_0}\right),$$

$\kappa = 0.40$ is the von Kármán constant, and Z_a is the reference level. Transfer functions F_M and F_T are defined by

$$F_M = 1 - \frac{\mathrm{Ri}_b}{M} \frac{2}{1 + \left(1 + \frac{2x}{M}\right)^{1/2}} \tag{7.3}$$

$$F_T = 1 - \frac{\mathrm{Ri}_b}{M} \frac{2}{1 + \left(1 + \frac{2x'}{M}\right)^{1/2}}, \tag{7.4}$$

where $M = \max(\mathrm{Ri}_c, \mathrm{Ri}_b + 1/a)$, $\mathrm{Ri}_c = 0.2$, and $a = 10$; $x = \zeta_a z_* d/H$, $x' = \zeta_a z_* d'/H$, $z_* = \max(Z_a - 10\ \mathrm{m}, 0)$; d and d' are parameters; and H is the height of the boundary layer. The expressions for F_M and F_T are empirical, selected for their ability to simulate the Wangara data (Delage 1988a,b).

Under unstable conditions, the functions for momentum and heat exchange at the surface are calculated as follows:

$$C_M = 1/\mathrm{FQ} \tag{7.5}$$

$$C_T = 1/\mathrm{FH}, \tag{7.6}$$

where

$$\mathrm{FQ} = \ln\left(\frac{Z_a + Z_0}{Z_0}\right) + \ln\left\{\frac{(X_0 + 1)^2(X_0^2 - X_0 + 1)^{1/2}(X_0^2 + X_0 + 1)^{3/2}}{(X + 1)^2(X^2 - X + 1)^{1/2}(X^2 + X + 1)^{3/2}}\right\} + \sqrt{3}\left\{\tan^{-1}\left(\sqrt{3}\,\frac{(X^2 - 1)X_0 - (X_0^2 - 1)X}{(X_0^2 - 1)(X^2 - 1) + 3XX_0}\right)\right\} \tag{7.7}$$

$$\mathrm{FH} = \ln\left(\frac{Z_a + Z_{0T}}{Z_{0T}}\right) + \frac{3}{2}\ln\left\{\frac{Y_0^2 + Y_0 + 1}{Y^2 + Y + 1}\right\} + \sqrt{3}\tan^{-1}\left(\sqrt{3}\,\frac{2(Y - Y_0)}{(2Y_0 + 1)(2Y + 1) + 3}\right), \tag{7.8}$$

and

$$X = \left\{1 - 40.0 \times (Z_a + Z_0) \times \frac{\kappa \times C_T \times \mathrm{Ri}_b}{C_m^2 \times Z_a}\right\}^{1/6}, \tag{7.9}$$

$$X_0 = \left\{1 - 40.0 \times Z_0 \times \frac{\kappa \times C_T \times \mathrm{Ri}_b}{C_m^2 \times Z_a}\right\}^{1/6}, \tag{7.10}$$

$$Y = \left\{1 - 40.0 \times (Z_a + Z_{0T}) \times \frac{\kappa \times C_T \times \mathrm{Ri}_b}{C_m^2 \times Z_a}\right\}^{1/3}, \tag{7.11}$$

$$Y_0 = \left\{1 - 40.0 \times Z_{0T} \times \frac{\kappa \times C_T \times \mathrm{Ri}_b}{C_m^2 \times Z_a}\right\}^{1/3}, \tag{7.12}$$

and where Z_{0T}, the thermal roughness length, is assumed equal to Z_0 for this study. Details for specification of the transfer functions FQ and FH are given in Delage (1988a,b).

REFERENCES

Chalikov, D., 1993: The parameterization of the wave boundary layer. *J. Phys. Oceanogr.*, submitted.

——, and M. Yu. Belevich, 1993: One-dimensional theory of the wave boundary layer. *Bound.-Layer Meteor.*, **63**, 65–96.

Charnock, H., 1955: Wind stress on a water surface. *Quart. J. Roy. Meteor. Soc.*, **81**, 639–640.

——, 1958: A note on empirical wind-wave formulae. *Quart. J. Roy. Meteor. Soc.*, **84**, 443–447.

de las Heras, M. M., and P. A. E. M. Janssen, 1992: Data assimilation with a coupled wind-wave model. *J. Geophys. Res.*, **97**(C12), 20 261–20 270.

Delage, Y., 1988a: The position of the lowest levels in the boundary layer of atmospheric circulation models. *Atmos.-Ocean*, **26**(3), 329–340.

——, 1988b: A parameterization of the stable atmospheric boundary layer. *Bound.-Layer Meteor.*, **43**, 365–381.

Dobson, F. W., and P. W. Vachon, 1994: The Grand Banks ERS-1 SAR wave spectra validation experiment: Program overview and data summary. *Atmos.-Ocean.*, **32**(1), 7–29.

Donelan, M. A., 1982: The dependence of the aerodynamic drag coefficient on wave parameters. *Proc. First Int. Conf. on Meteorology and Air–Sea Interaction of the Coastal Zone*, The Hague, Amer. Meteor. Soc., 381–387.

——, 1990: Air–sea interaction. *The Sea: Ideas and observations on Progress in the Study of the Seas.* Vol. 9, B. LeMéhauté and D. M. Hanes, Eds., Wiley-Interscience, 239–292.

——, F. W. Dobson, S. D. Smith, and R. J. Anderson, 1993: On the dependence of sea surface roughness on wave development. *J. Phys. Oceanogr.*, **23**, 2143–2149.

Geernaert, G. L., S. E. Larsen, and F. Hansen, 1987: Measurements of the wind stress, heat flux, and turbulence intensity during

storm conditions over the North Sea. *J. Geophys. Res.*, **92**(13), 127–139.

Hasselmann, K., 1962: On the nonlinear energy transfer in a gravity-wave spectrum. Part I. General theory. *J. Fluid Mech.*, **12,** 481–500.

——, 1974: On the spectral dissipation of ocean waves due to white-capping. *Bound.-Layer Meteor.*, **6,** 107–127.

——, and Coauthors (The WAMDI Group), 1988: The WAM model—A third generation ocean wave prediction model. *J. Phys. Oceanogr.*, **18,** 1775–1810.

Hsu, S. A., 1974: A dynamic roughness equation and its application to wind stress determination at the air–sea interface. *J. Phys. Oceanogr.*, **4,** 116–120.

——, 1986: A mechanism for the increase of wind stress (drag) coefficient with wind speed over water surface: A parametric model. *J. Phys. Oceanogr.*, **16,** 144–150.

Janssen, P. A. E. M., 1989: Wave-induced stress and the drag of air flow over sea waves. *J. Phys. Oceanogr.*, **19,** 745–754.

——, 1991: Quasi-linear theory of wind–wave generation applied to wave forecasting. *J. Phys. Oceanogr.*, **21,** 1631–1642.

Lionello, P., H. Günther, and P. A. E. M. Janssen, 1992: Assimilation of altimeter data in a global third generation wave model. *J. Geophys. Res.*, **C97,** 14 453–14 474.

Maat, N., C. Kraan, and W. A. Oost, 1991: The roughness of wind waves. *Bound.-Layer Meteor.*, **54,** 89–103.

Nordeng, T. E., 1991: On the wave age dependent drag coefficient and roughness length at sea. *J. Geophys. Res.*, **96**(C4), 7167–7174.

Smith, S. D., 1988: Coefficients for sea surface wind stress, heat flux, and wind profiles as a function of wind speed and temperature. *J. Geophys. Res.*, **93,** 15 467–15 472.

——, R. J. Anderson, W. A. Oost, C. Kraan, N. Maat, J. DeCosmo, K. B. Katsaros, K. L. Davidson, K. Bumke, L. Hasse, and H. M. Chadwick, 1992: Sea surface wind stress and drag coefficient: The HEXOS results. *Bound.-Layer Meteor.*, **60,** 109–142.

Snyder, R., F. Dobson, J. Elliott, and R. Long, 1981: Array measurements of atmospheric pressure fluctuations above surface gravity waves. *J. Fluid Mech.*, **102,** 1–59.

Toba, Y., and M. Koga, 1986: A parameter describing overall conditions of wave breaking whitecapping, sea-spray production and wind stress. *Oceanic Whitecaps,* E. C. Monahan and G. Mac Niocaill, Eds., D. Reidel, 37–47.

——, N. Iida, H. Kawamura, N. Ebuchi, and I. S. F. Jones, 1990: Wave dependence on sea-surface wind stress. *J. Phys. Oceanogr.*, **20,** 705–721.

Wang, L., and W. Perrie, 1993: Coupled wind-sea models and their impact on fluxes of momentum, sensible heat and latent heat. Canadian Tech. Rep. Hydrogra. and Ocean Sci., No. 149, 131 + viii pp.

Wu, J., 1980: Wind-stress coefficients over sea surface near neutral conditions: A revisit. *J. Phys. Oceanogr.*, **10,** 727–740.